SAND2019-11380J

# Photocurrent from Single Collision 14 MeV Neutrons in GaN and GaAs

Matthew J. Jasica, William R. Wampler, Gyorgy Vizkelethy, *Member, IEEE*, Brian D. Hehr, Edward S. Bielejec

***Abstract*—Accurate predictions of device performance in 14 MeV neutron environments relies upon understanding the recoil cascades that may be produced. Recoils from 14 MeV neutrons impinging on both gallium nitride (GaN) and gallium arsenide (GaAs) devices were modeled and compared to the recoil spectra of devices exposed to 14 MeV neutrons. Recoil spectra were generated using nuclear reaction modeling programs and converted into an ionizing energy loss (IEL) spectrum. We measured the recoil IEL spectra by capturing the photocurrent pulses produced by single neutron interactions with the device. Good agreement, with a factor of two, was found between the model and experiment under strongly-depleted conditions. However, this range of agreement between model and experiment decreased significantly when the bias was removed, indicating partial energy deposition due to cascades that escape the active volume of the device not captured by the model. Consistent event rates across multiple detectors confirm the reliability of our neutron recoil detection method.**

***Index Terms*—Gallium nitride, gallium arsenide, neutrons, photocurrent, radiation effects**

## I. Introduction

Gallium nitride (GaN) and gallium arsenide (GaAs) are of interest for applications in high radiation environments. Gallium nitride diodes have electrical properties favorable for high-power electronics, including their wide band gap, high critical breakdown field, and high displacement energy [1-3]. GaN power diodes have demonstrated a high resistance to decreases in breakdown voltage at proton fluences up to $10^{13}$ $cm^{-2}$ [4]. Gallium arsenide heterojunction bipolar transistors (HBTs) have also demonstrated superior resilience to gain degradation from neutron damage as compared to silicon bipolar junction transistors [5]. Recoil atoms from neutron interactions can produce displacement cascades and defects. Even single neutron collisions can result in undesirable effects such as gain degradation [6] or bit flips [7]. Simulating the effects of displacement damage in radiation environments relies on an accurate understanding of these recoil atom energy distributions. The recoil energy spectrum for a material can then be used to inform binary collision approximation (such as MARLOWE [8]) or molecular dynamics (such as LAMMPS [9])-based defect evolution models. Ultimately these defect models can be used to inform models that examine carrier transport and carrier-defect interactions in irradiated devices [10-12]

Devices operating in 14 MeV neutron environments will face different neutron-nuclei reaction channels and associated cross-sections than those operating in nuclear fission-relevant environments due to the different neutron energy spectrum. Consequentially, the neutron recoil energy spectrum will differ between the two environments, resulting in different defect profiles in the material. Fig. 1 demonstrates this contrast in damage cascade maps using MARLOWE [8]. A higher density of smaller defect clusters is observed for the lower energy fission neutrons, while the recoils from 14 MeV neutrons are less dense but single cascades affect a much larger spatial region. Because displacement damage effects are energy-dependent, modeling and testing devices operating in 14 MeV neutron environments require testing environments specific to these energies. We modeled the expected recoil spectra from 14 MeV neutrons in GaN and GaAs and compared these to experimental measurements of GaN vertical diodes and GaAs HBTs taken on the Sandia National Laboratory (SNL) DTn ion beam end station.

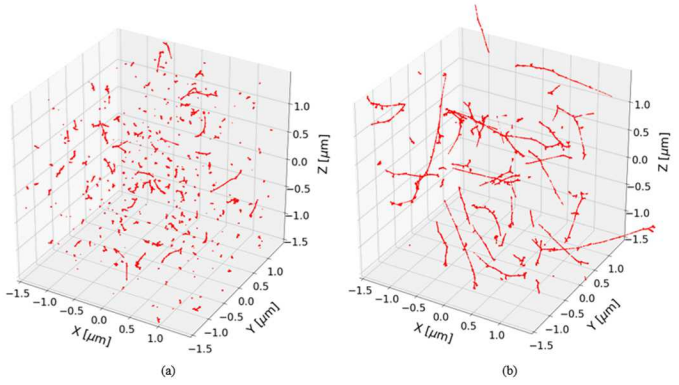


Fig. 1. Damage cascade maps calculated using MARLOWE for (a) the ACRR fission reactor [13] and (b) 14 MeV neutrons

Sandia National Laboratories is a multimission laboratory managed and operated by National Technology and Engineering Solutions of Sandia, LLC, a wholly owned subsidiary of Honeywell International, Inc., for the U.S. Department of Energy's National Nuclear Security Administration under contract DE-NA0003525.
This paper describes objective technical results and analysis. Any subjective views or opinions that might be expressed in the paper do not necessarily represent the views of the U.S. Department of Energy or the United States Government.
Matthew J. Jasica (mjjasic@sandia.gov), William R. Wampler (wrwampl@sandia.gov), Gyorgy Vizkelthy (gvizkel@sandia.gov), Brian D. Hehr (bdhehr@sandia.gov), and Edward S. Bielejc (esbiele@sandia.gov) are with Sandia National Laboratories, PO Box 5800, MS 1056, Albuquerque, NM, 87185, USA

## II. Model

Recoils from neutron collisions will deposit energy in the material through both displacement damage and IEL. Tthe experimental observation of recoil events is based only on the generation of charge carriers and photocurrent pulses by IEL as the recoil moves through the material. The approach here uses nuclear reactions calculation to determine a total recoil energy spectrum. This can be validated by converting this spectrum into an IEL spectrum, which can be directly compared to experiment.

First, neutron-induced total recoil energy calculations are performed using the EMPIRE [14] nuclear reaction modeling code. Total interaction cross sections at 14 MeV are taken from the Evaluated Nuclear Data File (ENDF) database [15], while relative reaction channel probabilities are preserved from the EMPIRE calculations. Contributions from multiple reaction channels are then processed together to form a single recoil spectrum corresponding to a single isotope (e.g. Ga-69). Average recoil spectra in composite materials, such as GaN or GaAs, are the average of the individual spectra as weighted by the computed number of collision events per unit volume per unit neutron fluence for each constituent isotope. These spectra are organized as the numerical fraction ΔN falling within each logarithmically-spaced bin ΔE. The recoil spectra for GaN and GaAs are shown in Fig. 2. The spectrum of each species indicates two energy peaks, representing the elastic scattering (lower energy) and non-elastic, primarily (n,n+γ) and (n,2n), (higher energy) channels. These recoil spectra only include energies deposited into the material from the primary recoil, and do not include energy deposited by any other charged products, such as protons or alpha particles. In the case of GaN and GaAs, the sum of the cross sections for elastic scattering, inelastic scattering, and (n,2n) reactions at 14 MeV is much larger than the summed cross section of channels producing light charged particles, such as (n,p) or (n,α), and any additional energy deposited by these charged particles can be safely ignored in our model. These calculations also yield the predicted number of collision events per unit volume per unit neutron fluence for 14 MeV neutrons with each device: 0.211 (collisions/cm$^3$)/(neutron/cm$^2$) for GaN and 0.145 (collisions/cm$^3$)/(neutron/cm$^2$) for GaAs.

Calculated recoil spectra are then converted into an IEL spectrum for comparison with experiment. The IEL fraction as a function of energy can be obtained from either theoretical the Norgett Robinson Torrens (NRT) model [16] or from the binary collision code SRIM-2013 [17]. (The NRT formulation directly yields the non-ionizing energy loss fraction. The IEL is then simply the remaining fraction.) Average values for the target Z and masses are used in the NRT formulation of the model. While this violates the original assumptions of a monatomic system as discussed within the NRT model, the results of this averaging are consistent with the SRIM formulation. These two fractions agree within 10-20% over the energy range of interest (shown in Fig. 3). Either the SRIM or NRT method is suitable for this model, as there is little significant difference in the resulting IEL spectra. For the purposes of this work, the NRT model was used. Scaling the recoil energies by the IEL fraction yields the IEL distribution of each material. The result is a downshift in energy from the recoil spectrum while relative probabilities $\frac{\Delta N}{\Delta E}$ remain unchanged, as shown in Fig. 4. This downshift is more pronounced at lower energies due to the greatly reduced IEL fraction.

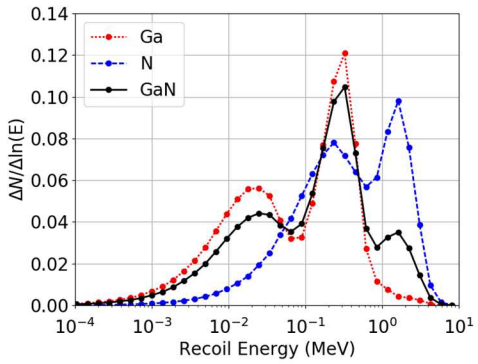


(a)

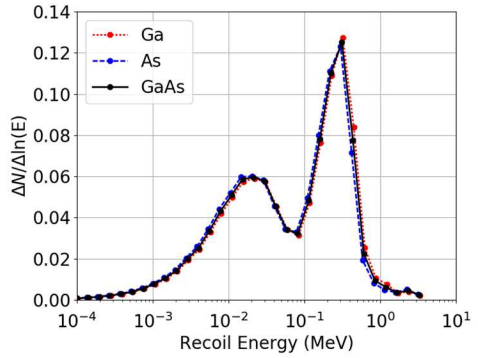


(b)

Fig. 2. Recoil spectra of 14 MeV neutrons on (a) GaN and (b) GaAs. The vertical scale is the fraction of events offering in each energy bin such that equal areas under the curve represent equal probabilities of occurrence.

## III. Experiment

The GaN devices used for this work were vertical power pn diodes approximately 150 μm in diameter with an n-layer 10 μm thick and a doping of ~2 × 10$^{16}$ cm$^{-3}$. The GaAs devices were npn HBTs. Specifically, the base-collector junction was studied in this work as this offered the largest target in the device for studying isolated recoils in GaAs. The collector thickness was 1.9 μm thick with an n-doping of ~6 × 10$^{15}$ cm$^{-3}$. Of specific interest for these experiments was the photocurrent response of the GaN or GaAs material to radiation, rather than the behavior of a vertical diode or HBT device. The devices selected have rather simple structures, enabling a more straightforward investigation of these material responses. The 14 MeV neutron irradiations were performed using the new DTn end station on the SNL Ion Beam Laboratory (IBL) High Voltage Engineering Europa (HVEE) implanter. A 270 kV $D_2^+$ beam (135 keV per deuteron) was accelerated into a thin film $TiT_2$ target. The beam current was ~50 μA as measured by a

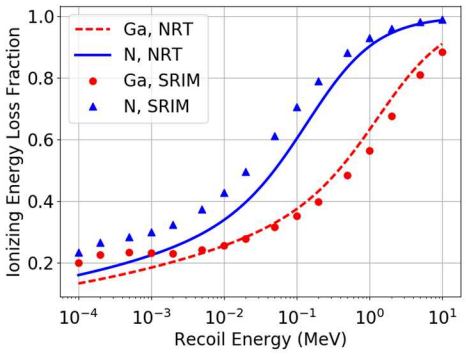


(a)

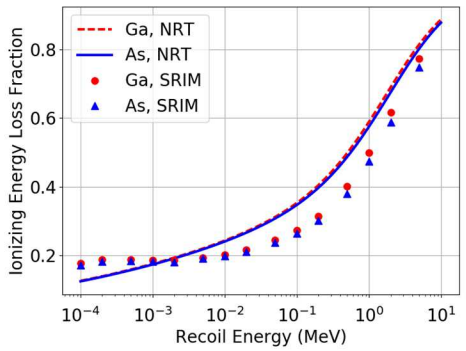


(b)

Fig. 3. IEL fractions calculated using the NRT model and SRIM for (a) GaN and (b) GaAs

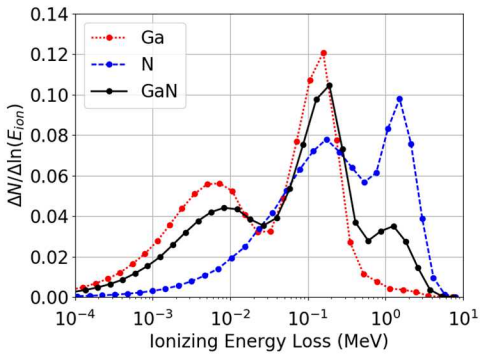


(a)

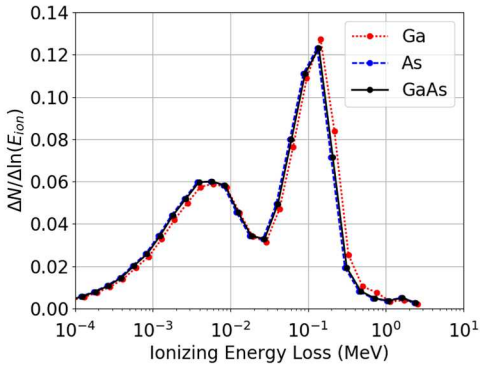


(b)

Fig. 4. IEL spectra due to 14 MeV neutrons on (a) GaN and (b) GaAs. The spectrum is the same as the recoil spectrum, downshifted in energy by the IEL fraction.

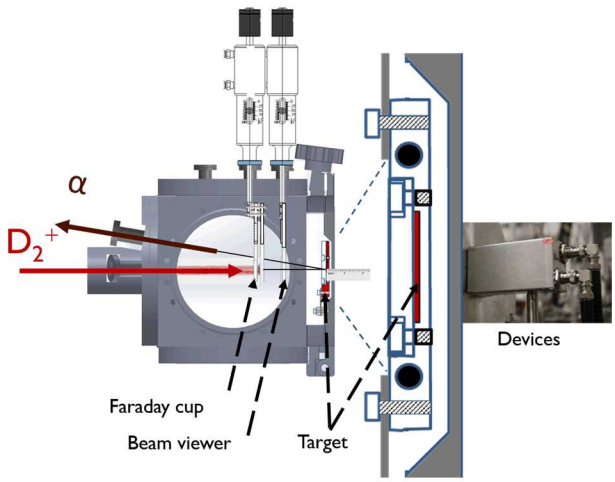


Fig. 5. Schematic of DTn end station with devices. Parts may be placed as close as 1 cm from the target.

Faraday cup. The neutron flux and fluence were calculated by measuring the rate of 3.5 MeV α particles produced by the T(d,n)α reaction with a silicon (Si) pin diode. Over time, D(d,p)T and will also occur as D is implanted into the sample, resulting in protons with 3.0 MeV. Only detected particles with energies near 3.5 MeV were counted, to reduce the influence of D-D reactions. These neutron flux measurements were in good agreement with the total integrated neutron fluence measured using Ni, Nb, and Zr foil activation dosimetry [18]. The design of the end station allows for experiments to be placed as close as 1 cm from the target to maximize the received neutron flux (see Fig. 5). The maximum number of neutrons produced by a single target on this end station is $1.6 \times 10^{15}$ neutrons, and the maximum fluence from a single target at 1 cm is $1.0 \times 10^{14}$ n/cm$^2$.

The IEL spectrum was determined by measuring the photocurrent pulses induced by individual neutron recoil events in the depletion regions of each material. The height of the pulse was proportional to the IEL in the depletion region. The GaN diode was reverse-biased across the p-n junction up to -100 V. The GaAs HBT was reverse-biased across the base-collector (B-C) junction up to -10 V while the emitter was left floating. The devices were encased in an aluminum box to minimize the pickup of ambient radio-frequency (RF) noise, and the box was located on the end station as close to the target as possible. Charge pulses were collected using a set of Ortec 142A preamplifiers. These pulses were then processed by an Ortec 671 or Ortec 672 spectroscopy amplifier. A Fast ComTec 7072 analog-digital converter in pulse-height analysis mode analyzed the signals and separated them into bins based on the pulse height (energy). Finally, this information interfaced with the data acquisition computer through a Fast ComTec MPA3 multi-parameter analyzer, which collects and saves the energy spectra. This system was calibrated using an Am-241 α particle source with an energy of 5.4 MeV and Si pin diode to determine the energy per channel for each device.

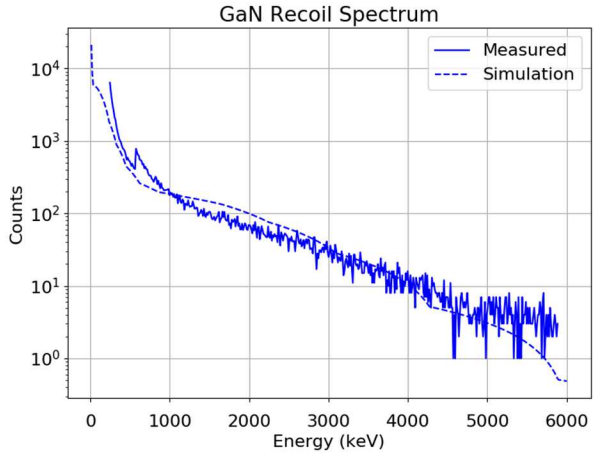


(a)

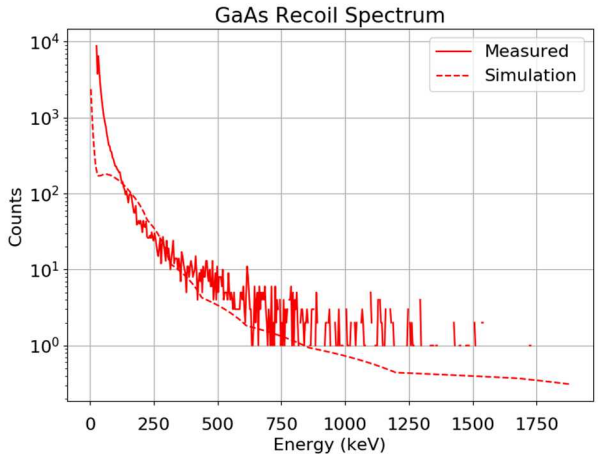


(b)

Fig. 6. Comparison of measured and simulated IEL spectra. (a) GaN reverse-biased to -100 V while receiving a fluence of $3.1 \times 10^{12}$ n/cm$^2$. (b) GaAs reverse-biased to -10 V while receiving a fluence of $6.3 \times 10^{12}$ n/cm$^2$.

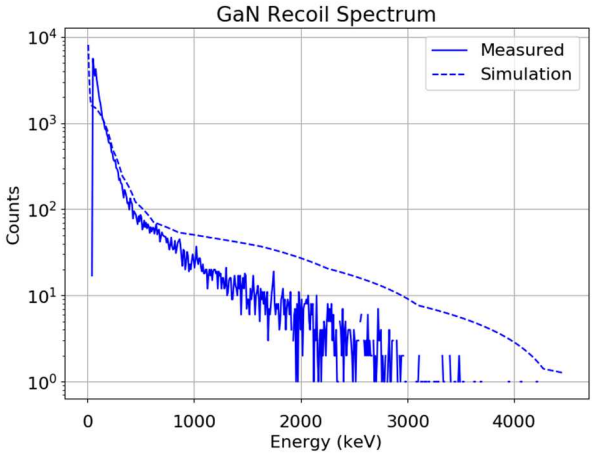


(a)

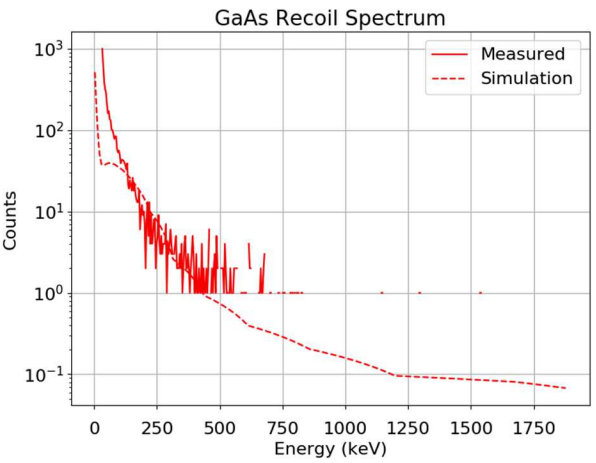


(b)

Fig. 7. Comparison of measured and simulated IEL spectra. (a) GaN with no bias while receiving a fluence of $3.9 \times 10^{12}$ n/cm$^2$. (b) GaAs with no bias while receiving a fluence of $3.0 \times 10^{12}$ n/cm$^2$.

## IV. RESULTS

The measured recoil IEL spectra for the GaN and GaAs devices biased to -100 and -10 V are shown in Figs. 6a and 6b. The depths of the depletion regions for these devices are 2.5 µm and 1.6 µm for the GaN and GaAs devices, respectively. The GaN spectrum represents a neutron fluence of $3.1 \times 10^{12}$ n/cm$^2$ collected over 174 hours of run time. The GaAs spectrum represents a neutron fluence of $6.3 \times 10^{12}$ n/cm$^2$ collected over 316 hours of run time. The simulated spectra are normalized to the number of counts in the measured spectra. Agreement within a factor of 2 is observed from 0.3 MeV to 5.5 MeV in GaN and from approximately 100 keV to 800 keV in GaAs. These represent the upper 29% and 25% of the IEL recoil cumulative distribution function (CDF) for GaN and GaAs, respectively.

IEL spectra were also taken with a 0 V bias on both the GaN and GaAs devices, shown in Figs. 7a and 7b. Both devices have depletion region depths of 0.6 µm under this bias. The GaN spectrum represents a fluence of $3.9 \times 10^{12}$ n/cm$^2$ collected over 176 hours of run time. The GaAs spectrum represents a neutron fluence of $3.0 \times 10^{12}$ n/cm$^2$ collected over 40 hours of run time.

Under conditions of no bias on the GaN, limited agreement within a factor of two was found between 0.25 MeV to 1.0 MeV. For conditions of no bias on the GaAs, agreement within a factor of two was limited between 100 keV and 500 keV. These ranges correspond to the 79% to 91% range of the GaN CDF and 75% to 98% of the GaAs CDF. Agreement within a factor of five extended up to 2.0 MeV for the GaN spectra and up to 850 keV for the GaAs spectra. The data were collected using multiple GaN diodes and GaAs HBTs. The resulting spectra are the sum of the spectra collected by the individual devices at each bias. The devices were inspected for potential degradation in performance (and charge collection efficiency) due to radiation exposure by measuring the current-voltage (I-V) curves of the devices before and after irradiation. No significant changes in the measured I-V characteristics were observed, indicating a minimal impact of displacement damage. However, device degradation due to fast neutrons has been observed in both GaN [4, 19-21] and GaAs [5, 22] devices at fluences higher than those received by the devices in this work, above $10^{13}$ n/cm$^2$.

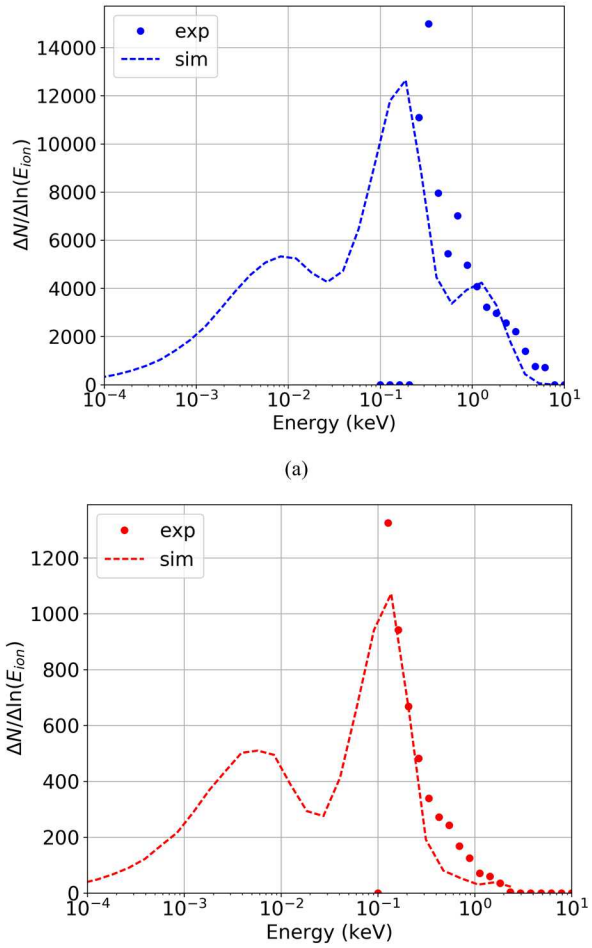


Fig. 8. Logarithmically-binned measured and modeled IEL spectra for (a) GaN reverse-biased to -100 V and (b) GaAs reverse-biased to -10 V.

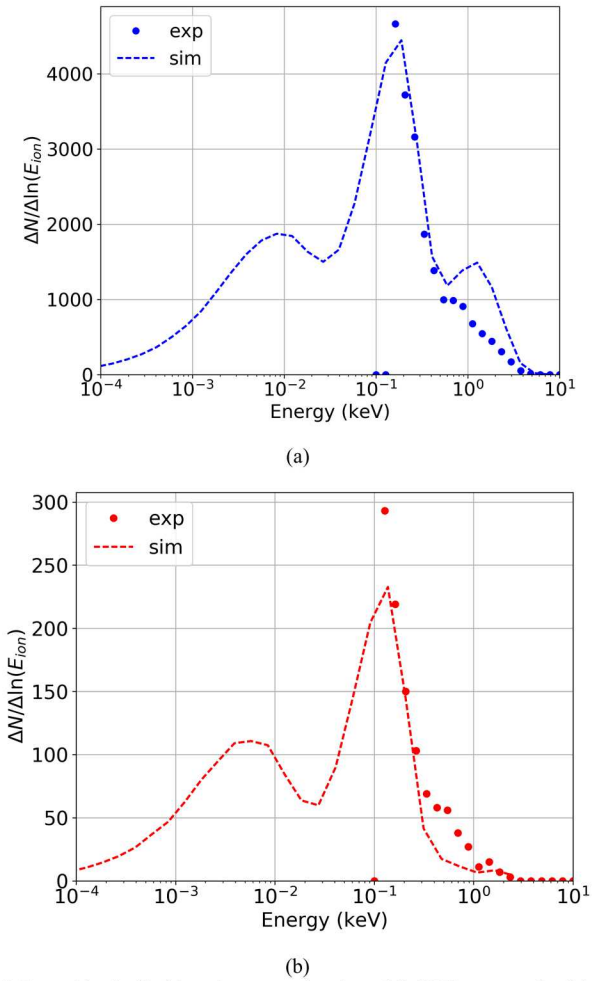


Fig. 9. Logarithmically-binned measured and modeled IEL spectra for (a) GaN with no bias and (b) GaAs with no bias.

## V. Discussion

Re-binning the measured data from Figs. 6 and 7 into logarithmically-spaced bins, as in Fig. 4, allows for a more obvious comparison between the originally calculated IEL spectra and the measured data. The re-binned data for the biased devices are shown in Fig. 8, and the re-binned data for the unbiased devices are shown in Fig. 9. In this manner, a more detailed look at the individual mechanisms responsible for the recoils can be probed. Due to the sensitivity of the experiment, the lower-energy Ga and As elastic recoil peaks cannot be detected. However, the data corresponding to non-elastic recoils from Ga and As (in GaN and GaAs) as well as elastic recoils from N (in GaN) have a strong match to the model. One feature not apparent in the linear energy scale representation of this data in Figs. 6 and 7 is a a systematic modeling underestimate of the experimental data by a factor of 2-3 from 500 keV to 1 MeV in the GaAs spectra. This feature appears under both biased and non-biased conditions. This may be due to lower-Z recoils or nuclear reaction products. Alternatively, this may be an artifact of the relatively low counting statistics in this energy regime. Higher counting statistics would enable a more definitive judgement on whether this peak was real.

The size of the active volume, controlled by the bias of the device, was found to have a significant effect on the collection of IEL and the match between model and experiment. The recoil will generate electron-hole pair over the entirety of its range, but only those generated in the active volume will be collected and registered as an energy pulse. The remainder of carriers generated in the field-free neutral region of the device recombine quickly and are not detected. When the GaN diode was biased to -100 V the depletion region was 2.5 μm in depth. This is comparable to the recoil range of a 5 MeV N recoil or 10 MeV Ga recoil in GaN, meaning that recoils up to these energies have the potential to deposit all or most of their IEL into the active volume, depending on the location of the recoil. (All recoil ranges were calculated using SRIM.) Decreasing the bias to 0 V shrinks the depletion region to 0.60 μm in depth, comparable to a 500 keV N recoil or 2 MeV Ga recoil in GaN. This is consistent with what is observed in Fig. 9a, where the peak due to non-elastic N recoils is not observed. Ions above these energies can create recoil cascades partially inside and partially outside the active volume, depositing only a fraction of their IEL into the active volume. The model assumes an infinite medium, such that all IEL is deposited into the material. The result of this would be that the modeled IEL spectrum

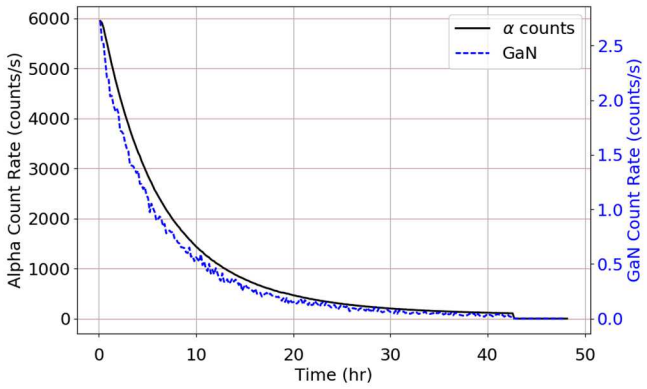


(a)

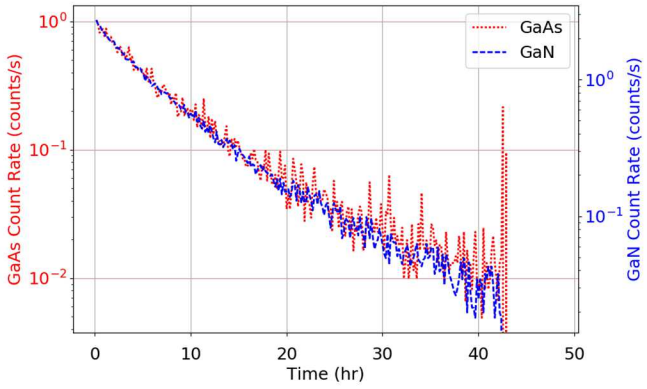


(b)

Fig. 10. Sample count rates over the lifetime of a single target. GaN energy cutoff below 200 keV and GaAs energy cutoff below 50 keV. A consistent exponential decay of all three devices is indicative of consistent neutron detection. (a) Alpha and GaN count rates. (b) GaN and GaAs count rates.

increasingly over-predicts the measured spectrum as the recoil energy increases, as seen in Fig. 7a. Similar behavior would be expected in the GaAs HBT. However, the number of particles in the spectrum (Fig. 7b) is too low to derive any meaning above 500 keV.

One of the challenges in collecting this data was the limited count rate for recoils in either the GaN or GaAs devices. In the GaN devices the detection rate was on the order of $10^{-8}$ recoils detected per n/cm$^2$ received. This rate in GaAs devices was on the order of $10^{-9}$ recoils detected per n/cm$^2$ received. This is attributed to both the small active volumes (i.e. depletion region) of the devices and the low reaction cross-sections for 14 MeV recoils with either GaN or GaAs. Despite these low count rates, we can have confidence in our counting statistics. Each spectrum contains approximately $5 \times 10^4$ counts (estimated error of ~0.4%), except for the 0 V GaAs case, which contained $5 \times 10^3$ counts (estimated error of ~1%). This allows us to place a high confidence in the lower energy portion of each spectrum where the spectrum remains continuous. While the upper energy channels contain on the order of 1 to 10 counts per channel, the total counts in the spectrum implies a correct order-of-magnitude response, even though the error of each individual channel is greater. Less confidence is placed in the shape of the spectrum where single counts appear in isolated channels, such as above 1250 keV in Fig. 6b.

This also ties in with the motivation behind the upper energy limits for these experiments. While the calculated recoil spectra for GaN goes up to 9.5 MeV, the gain settings of the experiment limited the upper energies to 6.0 MeV, where count rates were on the order of one or two counts per channel. Similarly, the experimental GaAs spectrum was limited to 1.9 MeV, though the model goes up to 4.0 MeV. Calculated detection rates for the maximum calculated energies were on the order of five to ten times lower than the rates at the maximum detected energies. Run times on the order of 1000 hours would be necessary to obtain adequate counting statistics to compare these portions of the spectrum to the model. Furthermore, good agreement between the model and experiment has already been found for the upper portions of each recoil spectrum. These upper energy limits correspond with the 99.996 percentile of the CDF for GaN and the 99.6 percentile for GaAs, and further experiments increasing the detected recoil energies would contribute little additional information to the findings here.

A known behavior of this experimental setup is the decrease in the neutron production rate over the lifetime of a single target due to tritium isotope exchange. The maximum hydrogen (D or T) concentration is determined by the stoichiometry and volume of the target. As D is implanted by the beam, it can diffuse through the target, replacing and ejecting tritium available for producing neutrons. This results in an exponential decay in the measured alpha signal, as seen in Fig. 10a.

It follows from this that the detected recoil rate must also obey the same exponential falloff in time. The raw GaN and GaAs spectra, integrated over all energies, on the contrary, did not always exhibit a similar signal decay with time, depending on the individual experiment setup. After excluding low amplitude pulses not from neutron recoils, the resulting recoil count rates were proportional to the neutron flux, as seen in Fig. 10a and 10b. These low energy cutoff values were ~200 keV for GaN and ~50 keV for GaAs. In general, the background count rate when the beam was blanked was low, limited to energies up to 60 keV for GaN and 22 keV for GaAs.

## VI. Conclusion

The energy spectra of recoils due to 14 MeV neutrons in both GaN and GaAs were modeled and compared to experiments using photocurrent pulses generated by the neutron recoils. We found good agreement at energies above 300 keV for GaN devices and between 100 keV and 750 keV for GaAs devices under reverse-biased conditions. The range of agreement dropped significantly when the devices were no longer biased. That the detection rates of the recoils were able to reproduce the time dependence of the alpha particles produced during neutron generation gives us confidence that the signals that we detected in the devices were neutron-induced recoils. Measurement of lower recoil energies is limited by the sensitivity of the nuclear instrumentation electronics as well as spurious low-energy signals associated with the neutron generation. Future modeling efforts will include the size of the depletion region and partial IEL deposition in the depletion region due to recoil cascades entering or exiting the depletion region.

## ACKNOWLEDGMENT

The authors would like to thank Bruce McWatters for operating the HVEE implanter for these experiments, Greg Pickrell (SNL) for providing GaN diodes, and Gary Patrizi (SNL) for providing GaAs HBTs.

## REFERENCES

[1] I. Vurgaftman and J. Meyer, "Electron Bandstructure Parameters," in Nitride Semiconductor Devices: Principles and Simulation, J. Piprek, Ed.: Wiley, 2007, pp. 13-48.

[2] A. M. Armstrong, A. A. Allerman et al., "High voltage and high current density vertical GaN power diodes," (in English), Electronics Letters, Article vol. 52, no. 13, pp. 1170-1171, Jun 2016.

[3] G. Sabui, P. J. Parbrook et al., "Modeling and simulation of bulk gallium nitride power semiconductor devices," AIP Advances, vol. 6, no. 5, p. 055006, 2016.

[4] M. P. King, A. M. Armstrong et al., "Performance and Breakdown Characteristics of Irradiated Vertical Power GaN P-i-N Diodes," IEEE Transactions on Nuclear Science, vol. 62, no. 6, pp. 2912-2918, 2015.

[5] G. A. Schrantz, N. W. v. Vonno et al., "Neutron irradiation effects on AlGaAs/GaAs heterojunction bipolar transistors," IEEE Transactions on Nuclear Science, vol. 35, no. 6, pp. 1657-1661, 1988.

[6] G. Vizkelethy, E. S. Bielejec, and B. A. Aguirre, "Stochastic Gain Degradation in III–V Heterojunction Bipolar Transistors Due to Single Particle Displacement Damage," IEEE Transactions on Nuclear Science, vol. 65, no. 1, pp. 206-210, 2018.

[7] C. A. Gossett, B. W. Hughlock et al., "Single event phenomena in atmospheric neutron environments," IEEE Transactions on Nuclear Science, vol. 40, no. 6, pp. 1845-1852, 1993.

[8] M. Robinson, "MARLOWE: computer simulation of atomic collisions in crystalline solids (Version 15b)," RSICC Code Package PSR-137, 2002.

[9] S. Plimpton, "Fast parallel algorithms for short-range molecular dynamics," Journal of computational physics, vol. 117, no. 1, pp. 1-19, 1995.

[10] S. Myers, P. Cooper, and W. Wampler, "Model of defect reactions and the influence of clustering in pulse-neutron-irradiated Si," Journal of Applied Physics, vol. 104, no. 4, p. 044507, 2008.

[11] W. R. Wampler and S. M. Myers, "Model for transport and reaction of defects and carriers within displacement cascades in gallium arsenide," Journal of Applied Physics, vol. 117, no. 4, p. 045707, 2015.

[12] W. R. Wampler, J. Lewis et al., "Validation of a model for stochastic variation in gain change of III-V heterojunction bipolar transistors from neutron irradiation," Sandia National Laboratories, Albuquerque, NM, Sandia Report SAND2016-12731, 2016.

[13] E. J. Parma, T. J. Quirk et al., "Radiation Characterization Summary: ACRR 44-Inch Lead-Boron Bucket Located in the Central Cavity on the 32-Inch Pedestal at the Core Centerline (ACRR-LB44-CC-32-cl)," Sandia National Laboratories, Albuquerque, NM, SAND2013-3406, 2013.

[14] M. Herman, R. Capote et al., "EMPIRE: Nuclear Reaction Model Code System for Data Evaluation," Nuclear Data Sheets, vol. 108, no. 12, pp. 2655-2715, 2007/12/01/ 2007.

[15] . National Nuclear Data Center Evaluated Nuclear Data File. Available: http://www.nndc.bnl.gov/exfor/endf00.jsp

[16] M. J. Norgett, M. T. Robinson, and I. M. Torrens, "Proposed Method of Calculating Displacement Dose-Rates," (in English), Nuclear Engineering and Design, vol. 33, no. 1, pp. 50-54, 1975.

[17] J. F. Ziegler, M. D. Ziegler et al., "SRIM–The stopping and range of ions in matter (2010)," vol. 268, no. 11-12, pp. 1818-1823, 2010.

[18] Standard Test Method for Measuring Neutron Fluence and Average Energy from 3H(d,n) 4He Neutron Generators by Radioactivation Techniques, ASTM E496-14e1, 2014.

[19] K.-X. Sun, M. Valles et al., "Gallium nitride (GaN) devices as a platform technology for radiation hard inertial confinement fusion diagnostics," Review of Scientific Instruments, vol. 89, no. 10, p. 10K113, 2018.

[20] A. Y. Polyakov, N. B. Smirnov et al., "Neutron Radiation Effects in Epitaxially Laterally Overgrown GaN Films," Journal of Electronic Materials, vol. 36, no. 10, pp. 1320-1325, 2007/10/01 2007.

[21] M. Rahman, A. Al-Ajili et al., "Super-radiation hard detector technologies: 3-D and widegap detectors," IEEE Transactions on Nuclear Science, vol. 51, no. 5, pp. 2256-2261, 2004.

[22] W. Braunschweig, T. Kubicki et al., "Investigation of the radiation damage of GaAs detectors by neutrons and photons," Nuclear Instruments and Methods in Physics Research Section A: Accelerators, Spectrometers, Detectors and Associated Equipment, vol. 372, no. 1, pp. 111-116, 1996/03/21/ 1996.